Tribology International 142 (2020) 105991

Contents lists available at ScienceDirect

Tribology International

journal homepage: http://www.elsevier.com/locate/triboint

# An assessment of gas power leakage and frictional losses from the top compression ring of internal combustion engines

R. Turnbull, N. Dolatabadi *, R. Rahmani, H. Rahnejat

*Wolfson School of Mechanical, Electrical and Manufacturing Engineering, Loughborough University, Leicestershire, LE11 3TU, UK*

ARTICLE INFO

*Keywords:*
Elastodynamics of piston compression ring
Blow-by
Gas leakage
Friction

ABSTRACT

A multi-physics integrated analysis of piston top compression ring of a high-performance internal combustion engines is presented. The effects of transient ring elastodynamics, thermal gas flow through piston crevices upon chamber leakage pressure and parasitic frictional losses are investigated. The multi-physics analysis comprises integrated flexible ring dynamics, ring-liner thermo-mixed hydrodynamics and gas blow-by, an approach not hitherto reported in literature. The predictions show close conformance to frictional measurements under engine motored dynamometric conditions. It is shown that power losses due to gas leakage can be as much as 6 times larger than frictional losses, which are usually considered as the main sources of inefficiency.

## 1. Introduction

The primary function of the piston compression ring is to provide a gas tight seal between the piston and the cylinder wall, preventing cylinder pressure loss and improve engine thermodynamic efficiency. Consequently, excessive interactions between the compression ring and cylinder liner promotes increasing friction and parasitic frictional power loss. Therefore, there are conflicting forms of power loss and operational efficiencies, which need to be considered whilst operating in the harsh mechanical and thermal loading conditions of internal combustion engines. Overall, up to 5% of the total IC engine losses are attributed to the piston compression ring conjunction with the cylinder [1].

Accurate prediction of energy losses is an important prelude for energy efficiency of the compression ring – cylinder liner interface, depending on the study of the effect of various parameters. Numerous predictive studies have been reported with varying degrees of complexity. Some Initial studies into the lubricant film thickness at piston reversals were conducted by Castleman [2] and Furuhama [3]. A one-dimensional (1D) solution was reported by Dowson et al. [4], who assumed a fully flooded conjunctional inlet under isothermal conditions with nominally smooth surfaces. This 1D solution was later extended for the case of lubricant starvation [5,6] and with mixed regime of lubrication [7,8].

Akalin and Newaz [8] showed good agreement between the results of their predictive model with experimental measurements of Furuhama and Sasaki [9]. A 2-dimensional solution of piston compression ring-cylinder liner contact is often required as the ring does not fully conform to the surface of the liner. Two-dimensional (2D) analyses were conducted, accounting for variable gap between the in-situ ring and the bore surface by Ma et al. [10] and Mishra et al. [11,12], with the latter showing better agreement with the measurements of Furuhama and Sasaki [9] than the 1D analysis in Ref. [8]. However, there were deviations from the measurements for frictional variation in transition from the compression to the power stroke at the top dead centre. The deviations from measurements are partly due to the fact that real cylinders are out-of-round, whilst most analyses assume the bore to be a perfect right circular cylinder [13]. Rahmani et al. [14] took into account the out-of-roundness of real cylinder liners as well as their axial profile. As the results they showed that the ring-bore contact remains in a mixed regime of lubrication during a large part of the power stroke in an engine cycle. The effect of an out-of-round bore on friction and blow-by was also studied by Piao and Gulwadi [15].

Tian et al. [16] noted the importance of the piston compression ring in reducing oil consumption without resorting to increased tension of the oil control ring [17], which typically compromises frictional performance. Takiguchi et al. [18] explored the effect of engine operating conditions on lubricant film formation at the top ring and second ring conjunctions of a diesel engine. Baelden and Tian [19] used finite element analysis (FEA) to study the effect of ring conformability and its structural deformation upon lubricant transport. The study also partly explains the difference between the experimental measurements of Furuhama and Sasaki [9] and the quasi-static analysis of Mishra et al. [12].

* Corresponding author.
*E-mail address:* N.Dolatabadi@lboro.ac.uk (N. Dolatabadi).

https://doi.org/10.1016/j.triboint.2019.105991
Received 1 July 2019; Received in revised form 18 September 2019; Accepted 30 September 2019
Available online 1 October 2019

**Nomenclature**

| | |
|---|---|
| $A$ | Apparent contact area $m^2$ |
| $A_1$ | Cross-sectional area of control volume normal to the flow $m^2$ |
| $A_2$ | Cross-sectional area of the ring $m^2$ |
| $A_g$ | End-gap area of the incomplete ring $m^2$ |
| $A_e$ | Real contact area between ring and liner $m^2$ |
| $C_d$ | Flow discharge coefficient |
| $C$ | Sutherland's number $kgm^{-1}s^{-1}K^{-0.5}$ |
| $E^{'}$ | Equivalent (reduced) Young's modulus of elasticity $N/m^2$ |
| $E_1$ | Young's modulus of elasticity of the liner material $N/m^2$ |
| $E_2$ | Young's modulus of elasticity of the ring material $N/m^2$ |
| $f_R$ | Radially applied force on the ring per unit length N/m |
| $f_m$ | Compressibility factor |
| $f_p$ | Tangentially applied force on the ring per unit length N/m |
| $G$ | Shear modulus of ring material $N/m^2$ |
| $h$ | Lubricant film thickness m |
| $h_s$ | Ring face axial profile m |
| $h_1$ | Width of the channel m |
| $I_2$ | Second area moment of inertia $m^4$ |
| $\mathbf{K}$ | Stiffness matrix N/m |
| $l$ | Connecting rod length m |
| $l_1$ | Land height m |
| $\mathbf{M}$ | Mass matrix kg |
| $p$ | Contact pressure distribution Pa |
| $P_{atm}$ | Atmospheric pressure Pa |
| $P_D$ | Downstream pressure Pa |
| $P_U$ | Upstream pressure Pa |
| $R$ | Gas constant $Jkg^{-1}K^{-1}$ |
| $R_2$ | Ring nominal radius m |
| $r$ | Crank pin radius m |
| $T$ | Piston top land temperature K |
| $T_U$ | Upstream temperature K |
| $T_0$ | Reference gas temperature K |
| $t$ | Time s |
| $U$ | Sliding velocity m/s |
| $u$ | Radial deflection m |
| $W_a$ | Asperity contact load N |
| $W_h$ | Hydrodynamic contact load N |
| $w$ | Circumferential in-plane deflection m |

*Greek symbols*

| | |
|---|---|
| $\alpha_0$ | Atmospheric pieso-viscosity coefficient $m^2/N$ |
| $\beta_0$ | Atmospheric thermo-viscosity coefficient |
| $\gamma$ | Thermal expansion coefficient for the lubricant $K^{-1}$ |
| $\gamma_s$ | Ratio of the specific heats |
| $\delta$ | Pressure induced localised (Hertzian) defection m |
| $\Delta$ | Global elastic deflection m |
| $\Delta\theta$ | Discretised interval in the circumferential direction rad |
| $\zeta$ | Coefficient of asperity shear strength |
| $\eta$ | Lubricant effective dynamic viscosity Pa. s |
| $\eta_0$ | Reference dynamic viscosity of gas Pa. s |
| $\eta_g$ | Gas dynamic viscosity Pa. s |
| $\theta$ | Circumferential angular position along the ring periphery rad |
| $\kappa$ | Average radius of curvature of asperites m |
| $\lambda$ | Stribeck lubricant film ratio |
| $\nu_1$ | Poisson's ratio of the liner material |
| $\nu_2$ | Poisson's ratio of the ring material |
| $\xi$ | Density of asperity peaks per unit area $1/m^2$ |
| $\rho$ | Lubricant density $kg/m^3$ |
| $\rho_0$ | Lubricant density at atmospheric conditions $kg/m^3$ |
| $\rho_2$ | Ring material density $kg/m^3$ |
| $\sigma$ | Combined RMS surface roughness m |
| $\tau$ | Viscous shear stress $N/m^2$ |
| $\tau_0$ | Characteristic Eyring shear stress $N/m^2$ |
| $\omega$ | Angular radiancy rad/s |

*Subscripts*

| | |
|---|---|
| $g$ | Combined |
| $ip$ | In-plane |
| $op$ | Out-of-plane |

*Abbreviations*

| | |
|---|---|
| 1D | One-dimensional |
| 2D | Two-dimensional |
| AFM | Atomic force microscope |
| BDC | Bottom dead centre |
| CDA | Cylinder de-activation |
| FDM | Finite difference method |
| FE | Finite element |
| FEA | Finite element analysis |
| ICE | Internal combustion engine |
| RMS | Root Mean Square |
| TDC | Top dead centre |

Although ring-bore conformability analysis was carried out in some of the above mentioned analyses, the approach was mostly quasi-static, not taking into account the elastodynamics of the thin compression ring under transient conditions, with modal responses in the radial direction (in-plane dynamics) and in the axial direction of the bore (out-of-plane ring dynamics). Baker et al. [20–22] were able to show considerable improvements in numerical predictions through progressive improvements to their elastic ring model, culminating in a 3-dimensional elastodynamic ring. In fact, it has also been shown that ring dynamics plays a significant role in affecting engine oil consumption, oil degradation, piston ring and liner wear, blow-by, and unburnt hydrocarbon products as well as friction [16,20–22]. The frictional and wear performance can have implications on the coated surfaces for these conjunctions [23]. Piston ring-cylinder liner friction and wear can also cause unstable idle speed in engines due to any gas leakage [24]. Tian et al. [16] also numerically verified the experimental results of Furuhama et al. [25] for the top ring flutter under high-speed, low-load operating conditions. Namazian and Heywood [26] showed that reduced ring friction can also lead, not only to ring flutter, but also ring jump with associated loss of chamber pressure. Therefore, ring dynamics is related to conjunctional friction (as one of the boundary conditions), resulting in power loss, blow-by and associated unburnt hydrocarbons at the piston ring crevices. Baker et al. [27] also took into account the effect of ring dynamics in ring jump, loss of chamber pressure and blow-by. Other studies, taking into account the effect of ring dynamics, include that of Ejakov et al. [28] who presented the flexibility of the ring in a gas blow-by model using flexible dynamics of a straight beam as an approximation. Tian [29,30] also developed a finite element model of a curved beam in their study of gas blow-by, oil transport and ring-liner lubrication. Therefore, clearly, Ring dynamics can significantly affect the tribological behaviour of the contact through variations in the contact load, contact geometry and kinematics. Therefore, a better understanding of the dynamics of piston compression ring dynamic is a prerequisite for a more accurate power loss analysis. Reasonable agreement between numerical predictions and experimental measurements of piston compression ring frequency response was observed by Turnbull et al.

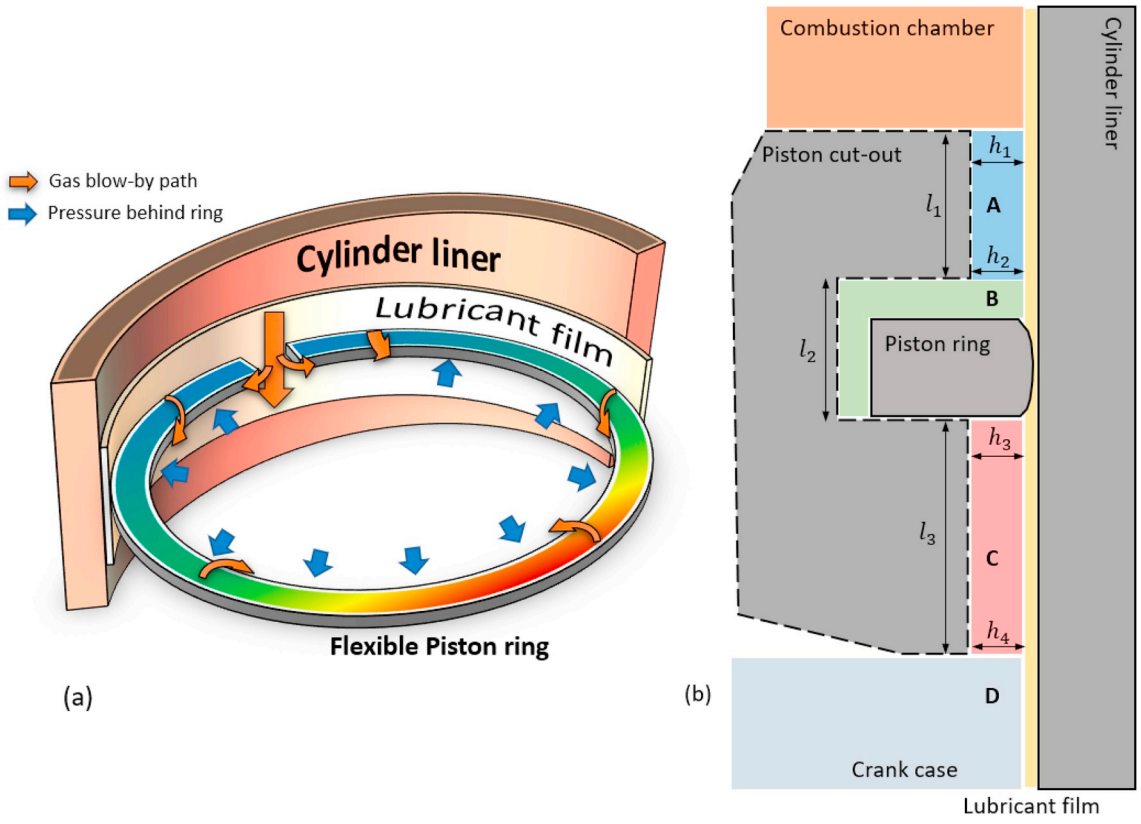


**Fig. 1.** (a) 3D representation of the flexible piston ring model and (b) schematic representation of the control volumes in the gas blow-by model.

[31] using various frequency sweeps. The model was later developed into a generic equivalent mass and stiffness matrix method which directly embedded the effect of ring curvature for a variety of boundary conditions [32]. The reported method increased the accuracy of predictions when compared with experimental measurements, capturing higher order frequency responses, not observed previously.

Accurate prediction of piston ring behaviour relies on complex and integrative analysis of ring dynamics, structural deformation, tribological contacts, lubricant rheology, gas flow dynamics, heat generation and flow through ring-piston ring-land crevices. Such an approach is essential in the trade-off between ring frictional losses and power losses due to loss of sealing, which is the integrated approach presented in this paper, and not hitherto reported in the open literature.

## 2. Methodology

### 2.1. Tribological model

Piston ring-cylinder liner lubricated conjunction is modelled using two-dimensional Reynolds' equation for a compressible piezo-viscous lubricant as:

$$\frac{\partial}{\partial x}\left(\frac{\rho h^3}{6\eta}\frac{\partial p}{\partial x}\right)+\frac{\partial}{\partial y}\left(\frac{\rho h^3}{6\eta}\frac{\partial p}{\partial y}\right)=\frac{\partial(\rho U h)}{\partial x}+2\frac{\partial(\rho h)}{\partial t} \tag{1}$$

where, $\rho$, $\eta$, $h$, $p$, $U$ are the lubricant density, dynamic viscosity, film thickness and shape, generated contact pressure distribution and the sliding velocity. Any side leakage of the lubricant in the lateral (circumferential direction of the bore) is ignored, owing to the low lubricant flow through the conjunction. Therefore, the lubricant film thickness varies in a transient manner in an engine cycle as:

$$h(x,y,t)=h_m(t)+h_s(x)+\Delta(y,t)+\delta(x,y,t) \tag{2}$$

Therefore, the lubricant film thickness is a function of ring face-width profile, $h_s$, and the global (elastic/structural) deflection of the ring, $\Delta$, and any pressure-induced localised (Hertzian-type) deflection of the ring-liner interface, $\delta$. The in-plane ring dynamics affects the minimum film thickness, $h_m$ through $\delta$. Mishra et al. [11,12] showed that the pressure-induced localised deformation, $\delta$, is usually negligible in typical gasoline engine road vehicles due to relatively low to medium range hydrodynamic contact pressures of the order of few tens of MPa between the ring and the liner.

The overall sliding velocity of the compression ring equates the piston velocity regardless of small ring flutter within the piston groove. Thus, the sliding velocity can be determined using piston kinematics as [33]:

$$U(\phi)=-r\omega\sin\phi\left\{1+\cos\phi\left[\left(\frac{l}{r}\right)^2-\sin^2\phi\right]^{-\frac{1}{2}}\right\} \tag{3}$$

where, $r$, $l$, $\phi$ and $\omega$ are the crank-pin radius, the connecting rod length, crank angle and the crankshaft angular velocity respectively.

Lubricant density and dynamic viscosity alter with generated pressure and temperature. The density variation with pressure and temperature is given by modified Dowson and Higginson [34] relationship to include temperature [35]:

$$\rho=\rho_0\left[1+\frac{6\times10^{-10}(p-P_{atm})}{1+1.7\times10^{-9}(p-P_{atm})}\right][1-\beta(T-T_0)] \tag{4}$$

where, $\rho_0$ and $\gamma$ are lubricant density at atmospheric conditions and the coefficient of thermal expansion of the lubricant. Houpert [36] proposed a relationship for lubricant dynamic viscosity variation with pressure and temperature, based on the original work of Roeland [37]:

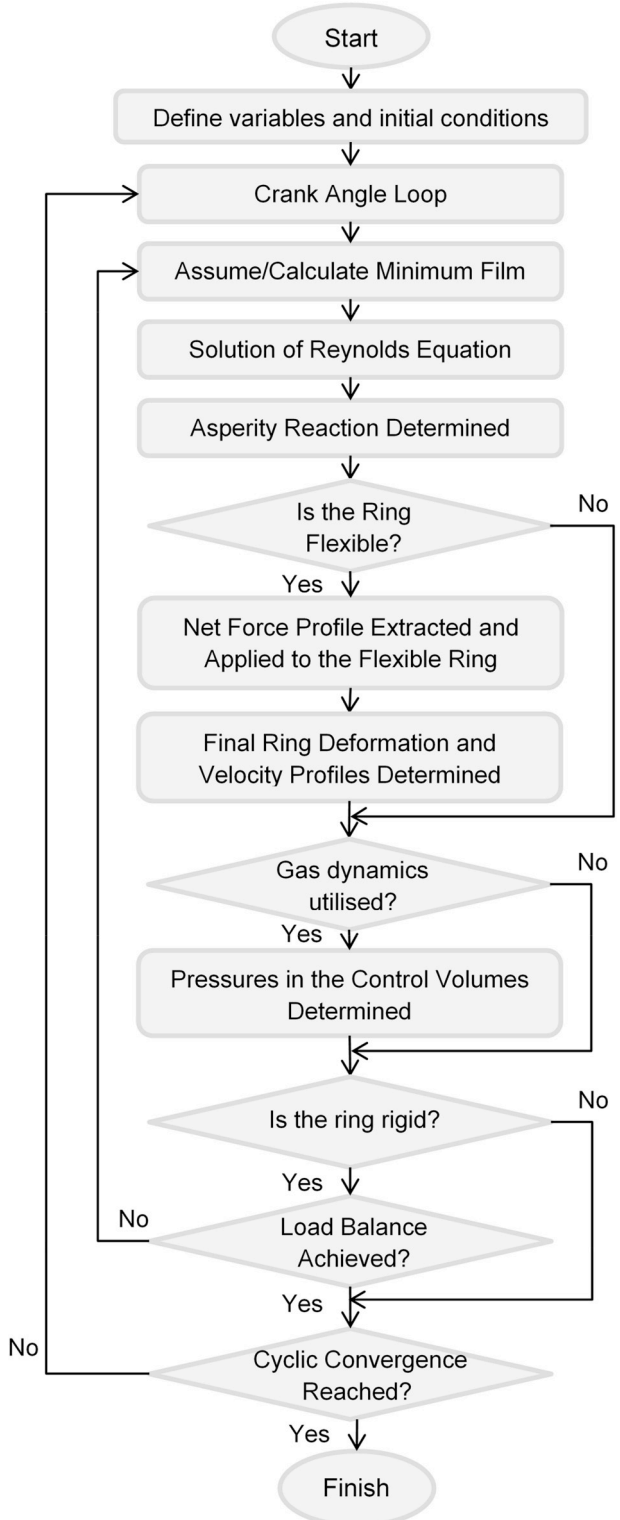


**Fig. 2.** Flow chart of the integrated analysis method.

**Table 1**
Engine and lubricant specifications.

| Parameter | Value | Unit |
|---|---|---|
| Compression ring material | Steel | – |
| Liner base material | Steel | – |
| Lubricant density at 110 °C | 806 | kg/m$^3$ |
| Lubricant viscosity at 110 °C | 10 | mPa.s |
| Coefficient of thermal expansion | $6.4 \times 10^{-4}$ | K$^{-1}$ |
| Pressure-viscosity coefficient | $2 \times 10^{-8}$ | Pa$^{-1}$ |
| Temperature-viscosity coefficient | 0.04 | K$^{-1}$ |
| Surface roughness parameter ($\xi\kappa\sigma$) | 0.00369 | – |
| Roughness slope parameter ($\sigma/\kappa$) | 0.0854 | – |
| Coefficient of asperity shear strength | 0.17 | – |
| Young's modulus of the liner | 203 | GPa |
| Poisson's ratio of the liner | 0.3 | – |
| Young's modulus of the ring | 203 | GPa |
| Poisson's ratio of the ring | 0.3 | – |
| Ring face-width | 1.15 | *mm* |
| Ring radial thickness | 3.5 | *mm* |
| Ring end gap size (free ring) | 10.5 | *mm* |
| Ring material density | 7850 | kg/m$^3$ |

$$\eta = \eta_0 \exp\left\{ \ln\left(\frac{\eta_0}{\eta_\infty}\right)\left[\left(\frac{T-138}{T_0-138}\right)^{-S_0}\left(1+\frac{p-p_{atm}}{C_p}\right)^{Z}-1\right]\right\} \tag{5}$$

where, $\eta_0$ is the lubricant dynamic viscosity at atmospheric conditions. Constants $\eta_\infty$ and $C_p$ are $6.31 \times 10^{-5}$ Pa s and $1.98 \times 10^{8}$ Pa respectively, whilst the lubricant piezo-viscosity and thermo-viscosity indices are determined as:

$$Z = \frac{\alpha_0 C_p}{\ln\left(\frac{\eta_0}{\eta_\infty}\right)}, \quad S_0 = \frac{\beta_0 (T_0 - 138)}{\ln\left(\frac{\eta_0}{\eta_\infty}\right)} \tag{6}$$

where, $\alpha_0$ and $\beta_0$ are atmospheric piezo-viscosity and thermo-viscosity coefficients.

Once the pressure distribution is determined through Reynolds equation, the hydrodynamic load carrying capacity can be determined as:

$$W_h = \int\int p \, dA \tag{7}$$

The lubricant film thickness decreases during piston reversals with diminishing sliding velocity and the rate of entrainment of the lubricant into the ring-bore conjunction. This momentary cessation of lubricant entrainment means that the conjunction is subject to mixed or boundary regime of lubrication, where some of the load is carried by the direct interaction of asperity peaks on the counter faces (the ring and the liner). Assuming a Gaussian distribution of asperities height for a out-in engine cylinder on the cross-hatched surface plateau, then asperity contact load can be predicted using Greenwood and Tripp [38] model as:

$$W_a = \frac{16\sqrt{2}}{15}\pi(\xi\kappa\sigma)^2\sqrt{\frac{\sigma}{\kappa}}E^{`}AF_{5/2}(\lambda) \tag{8}$$

where, $\xi$, $\kappa$ and $\sigma$ are the asperity distribution per unit contact area, the average asperity tip radius of curvature and the composite surface roughness of the contiguous surfaces. The Stribeck's lubricant film ratio, $\lambda$, is defined as $\lambda = h/\sigma$. $A$ is the apparent contact area and $F_{5/2}$ is a statistical function of lubricant film ratio approximated by a fifth order polynomial as [39]:

$$F_{5/2}(\lambda) = \begin{cases} -0.0046\lambda^5 + 0.0574\lambda^4 - 0.2958\lambda^3 + 0.7844\lambda^2 - 1.0776\lambda + 0.6167; & \text{for } \lambda \le \lambda_c = 2.224 \\ 0 \quad ; \quad \text{for } \lambda > \lambda_c = 2.224 \end{cases} \tag{9}$$

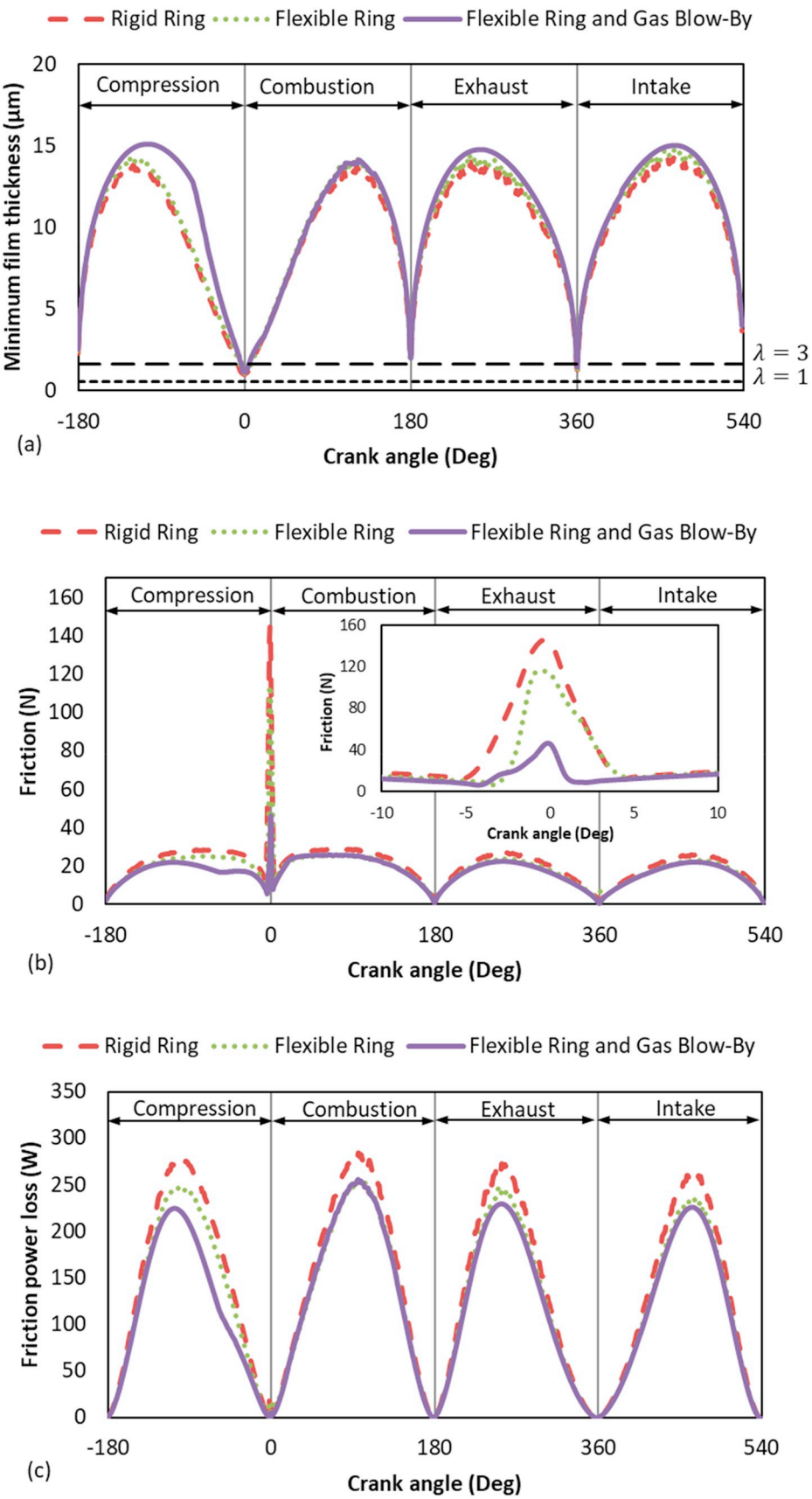


**Fig. 3.** The predicted results for (a) the minimum film thickness, (b) contact friction, and (c) power loss of a rigid-body ring, flexible ring and a flexible ring with compressible gas flow.

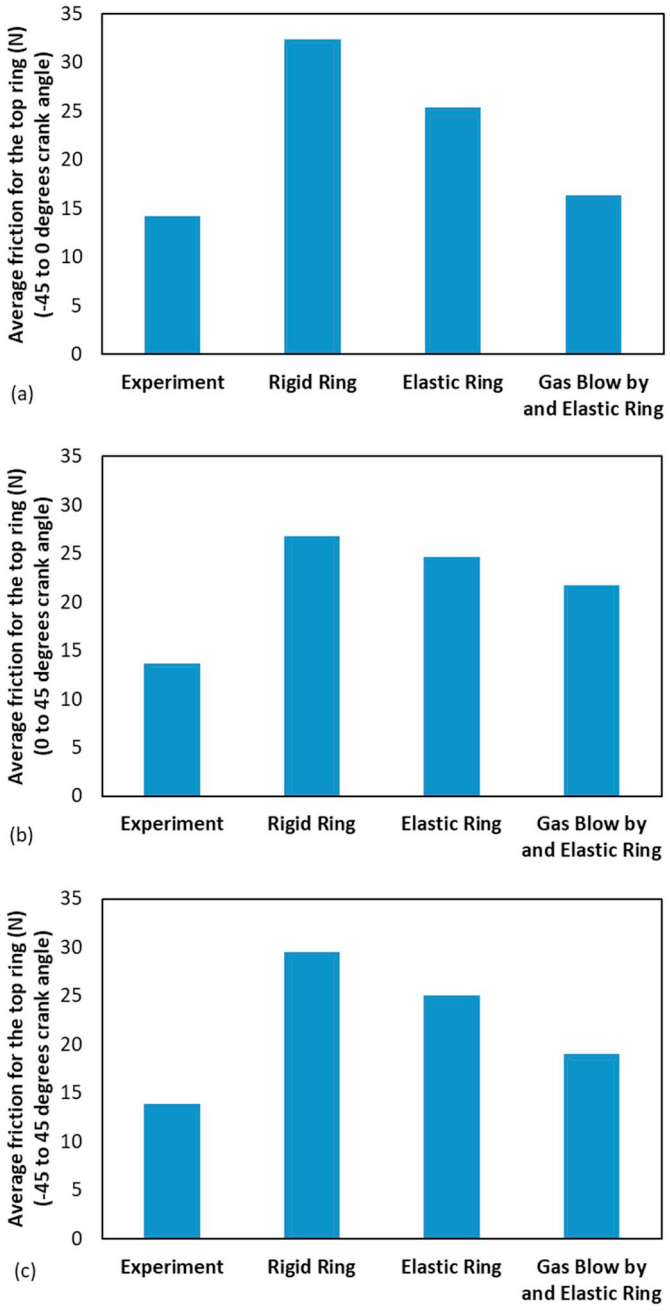


**Fig. 4.** Measured and predicted average friction for the top ring: (a) in the −45°–45° crank angle region (b) in −45°–0° crank angle region in the compression stroke (c) in 0°–45° degrees crank angle in the combustion stroke.

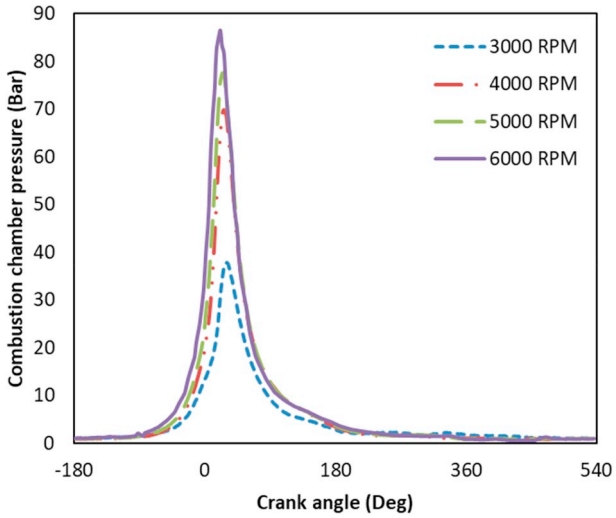


**Fig. 5.** The measured cylinder pressures at various engine speeds for the Honda CRF450R.

$$\frac{1}{E^{*}} = \frac{1-\nu_1^2}{E_1} + \frac{1-\nu_2^2}{E_2} \tag{10}$$

where, subscripts 1 and 2 refer to the cylinder liner and the piston compression ring respectively.

The generated contact friction comprises viscous shear of thin lubricant film and boundary friction as the result of interactions of asperity pairs protruding out of the thin lubricant film. Therefore, the total friction becomes:

$$f_t = f_v + f_b \tag{11}$$

Boundary friction is evaluated using [38]:

$$f_b = \tau_0 A_e + \zeta W_a \tag{12}$$

where, $\tau_0$ is the limiting Eyring shear stress of the lubricant, beyond which non-Newtonian tractive behaviour occurs [40,41], and $\zeta$ is the coefficient of asperity shear strength measured using an atomic force microscopy (AFM) in lateral force mode [40,42]. The real area of contact area (as opposed to the apparent area of contact $A$) $A_e$, represents the effective asperity contact area as:

$$A_e = \pi^2(\xi\kappa\sigma)^2 A F_2(\lambda) \tag{13}$$

where, $F_2$ is a statistical function of the Stribeck lubricant film ratio, $\lambda$, and is fitted to a 5th order polynomial [39] as:

$$F_2(\lambda) = \begin{cases} -0.0018\lambda^5 + 0.0281\lambda^4 - 0.1728\lambda^3 + 0.5258\lambda^2 - 0.8043\lambda + 0.5003; & \text{for } \lambda \le \lambda_c = 2.295 \\ 0 \quad ; & \text{for } \lambda > \lambda_c = 2.295 \end{cases} \tag{14}$$

The effective (equivalent) Young's modulus of elasticity of the contact pair, $E^{*}$, is obtained, based on moduli of elasticity and Poisson's ratios, $\nu$, of the two surface materials as:

Viscous friction occurs for the wetted part of the contact area due to hydrodynamic shear as:

$$f_v = \tau(A - A_e) \tag{15}$$

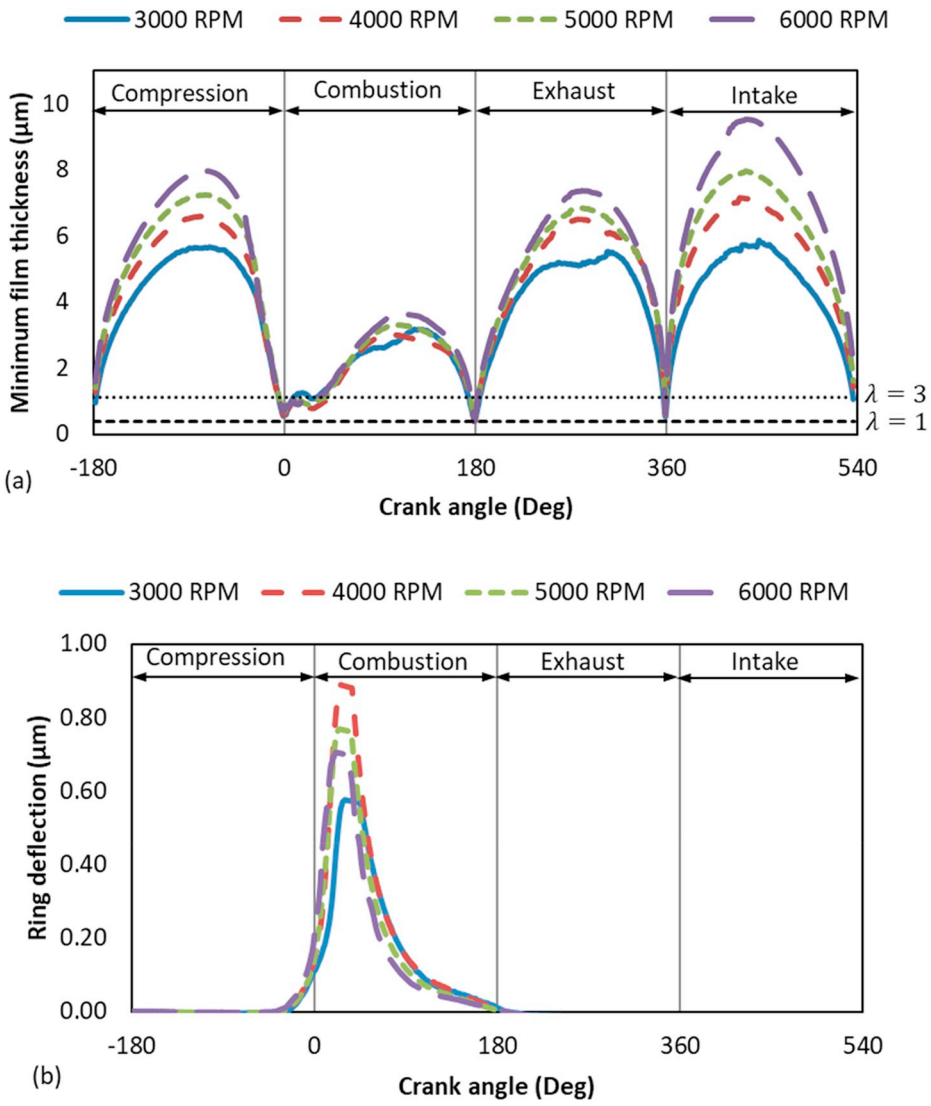


**Fig. 6.** (a) The minimum film thickness variations with crank angle at various engine speeds (b) ring deflection at the minimum film thickness with crank angle at various engine speeds.

The viscous shear stress of the lubricant, $\tau$, varies with contact pressure as well as lubricant viscosity and film thickness [14]:

$$\tau = \left| \pm \frac{h}{2} \vec{\nabla} p + \vec{\nabla} \frac{\eta}{h} \right| \tag{16}$$

Friction generates heat in the contact area which supplements the heat due to combustion. These heat sources increase the temperature of the contacting surfaces; liner and the ring, as well as the lubricant film. A fairly detailed thermal model is required. Morris et al. [43] reported a thermo-mixed lubrication analysis of the piston ring conjunction, using a control volume thermal network model for the compression ring-cylinder liner conjunction. They showed that the contact temperature is primarily controlled by the cylinder liner temperature with only a few degrees temperature rise due to viscous and boundary contact friction. This finding is confirmed by the experimental and numerical analysis of others [44,45]. Therefore, the contact temperature is taken as that measured from the cylinder liner surface by Furuhama et al. [46] for a small engine, representative of that studied in the current study.

### 2.2. Gas blow-by model

The combustion gases flow into the crevices between piston ring, piston grooves and the cylinder liner as the cylinder pressure rises. Following the method presented by Baker et al. [22], a thermal flow control volume method is used to predict the mass flows through the boundaries of each crevice (Fig. 1).

The generated contact pressure for the piston ring is determined by the trapped mass behind the ring (i.e. the control volume B). The mass flow rate through each crevice can be modelled assuming a laminar isothermal flow through an equivalent narrow channel. The flow rate through the incomplete circular ring end-gap can be evaluated by a laminar flow through an equivalent orifice. Namazian and Heywood [26] verified experimentally that Reynolds number is relatively low in these crevices (Re ≈ 10). Therefore, the laminar flow assumption is valid for the gas blow-by problem. Therefore, the mass flow rate from the combustion chamber to the control volume A (Fig. 1) can be approximated as [14,50]:

$$\dot{m}_1 = \frac{A_1 h_1^2}{24 l_1} \frac{1}{\eta_g R T} \left( P_{Ch}^2 - P_A^2 \right) \tag{17}$$

where, $\dot{m}_1$ is the mass flow rate between the control volumes A and B. Parameters $h_1$, $l_1$ and $A_1$ are the width, the length and the cross-sectional area normal to the flow of channel respectively. $R$, is the ideal gas constant and upstream temperature, $T$, is approximated to the piston

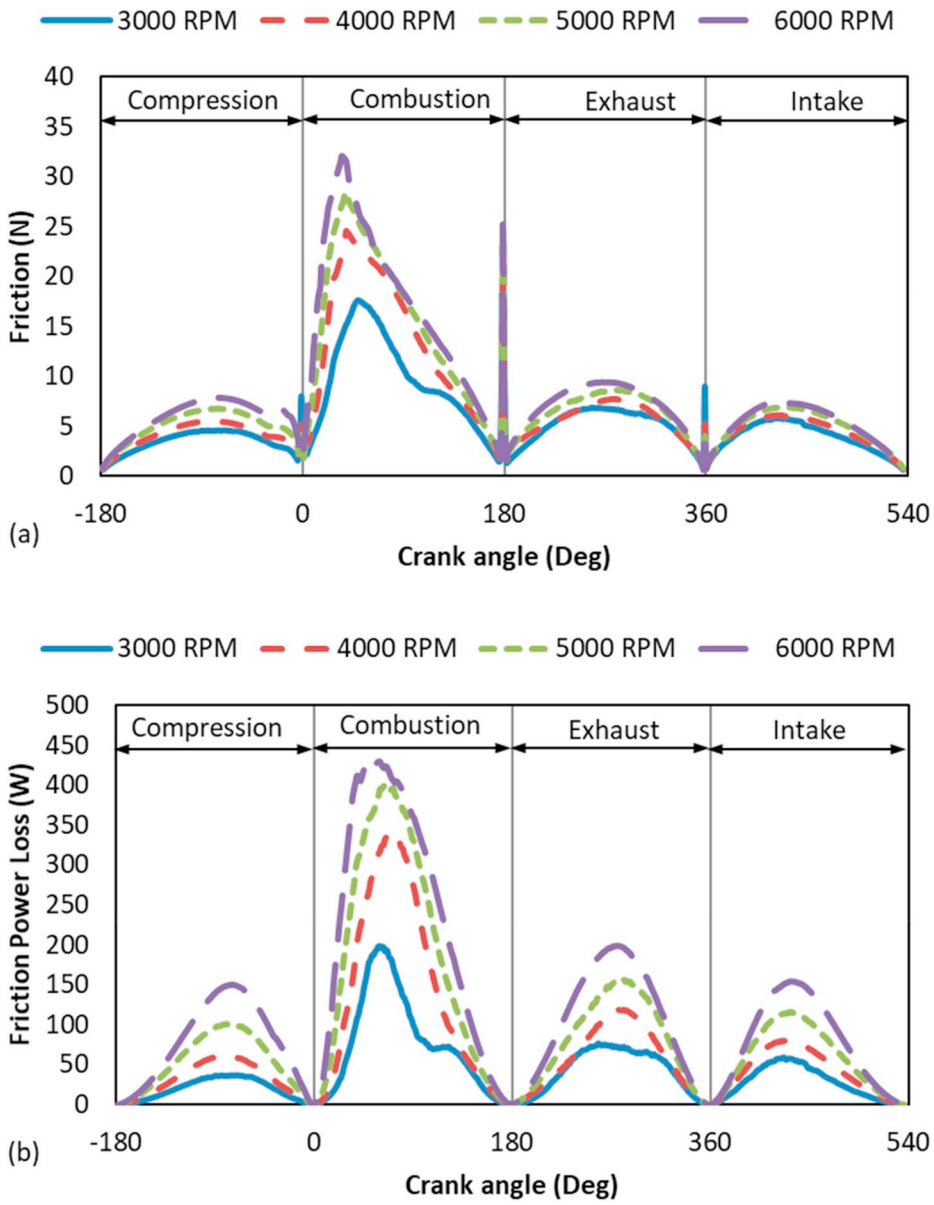


**Fig. 7.** Compression ring (a) friction at various engine speeds (b) power loss at various engine speeds.

top-land temperature. Namazian and Heywood [26] showed that the temperature of the gas flow in crevices is only a few degrees higher than that of the contiguous boundary surfaces. $P_A$ and $P_B$ are the gas pressures in the control volumes A and B respectively. The viscosity of the gas, $\eta_g$, is evaluated as [47]:

$$\eta_g = \eta_0 \frac{(T_0 + C)}{(T + C)} \left(\frac{T}{T_0}\right)^{3/2} \tag{18}$$

where, $\eta_0$ is the dynamic viscosity of the gas at the reference temperature, $T_0$, and the constant $C$ is the Sutherland's number, described in Ref. [48].

The mass flow rate through the ring end-gap is estimated assuming an isentropic flow through an equivalent orifice [47], thus:

$$\dot{m}_{eg} = C_d A_g \frac{P_U}{\sqrt{RT_U}} f_m \tag{19}$$

where, $C_d$ and $A_g$ are the coefficient of discharge and the ring end-gap area respectively. The orifice upstream temperature, $T_U$, equals the temperature of the control volume A. The compressibility factor, $f_m$, varies with the upstream pressure, $P_U$, downstream pressure, $P_D$, and the ratio of specific heats, $\gamma_s$ [26,47]:

$$f_m = \begin{cases} \gamma_s^{\frac{1}{2}} \left(\frac{2}{\gamma_s + 1}\right)^{\frac{\gamma_s + 1}{2(\gamma_s - 1)}}, & \frac{P_D}{P_U} > \left(\frac{2}{\gamma_s + 1}\right)^{\frac{\gamma_s}{(\gamma_s - 1)}} \\ 0.85 - 0.25\left(\frac{P_D}{P_U}\right)^2, & \frac{P_D}{P_U} \leq \left(\frac{2}{\gamma_s + 1}\right)^{\frac{\gamma_s}{(\gamma_s - 1)}} \end{cases} \tag{20}$$

The coefficient of discharge, $C_d$, is given as:

$$C_d = 0.85 - 0.25\left(\frac{P_D}{P_U}\right)^2 \tag{21}$$

Fuel energy is transformed into mechanical power in an internal combustion engine. Some of this power is dissipated in the form of friction and heat at the piston rings' conjunctions with the cylinder liner and partly through the work done in compression of combustion gases in the various crevices. For isentropic flows, the specific work done per unit mass on the compressible gas, $W_d$, can be approximated as [49]:

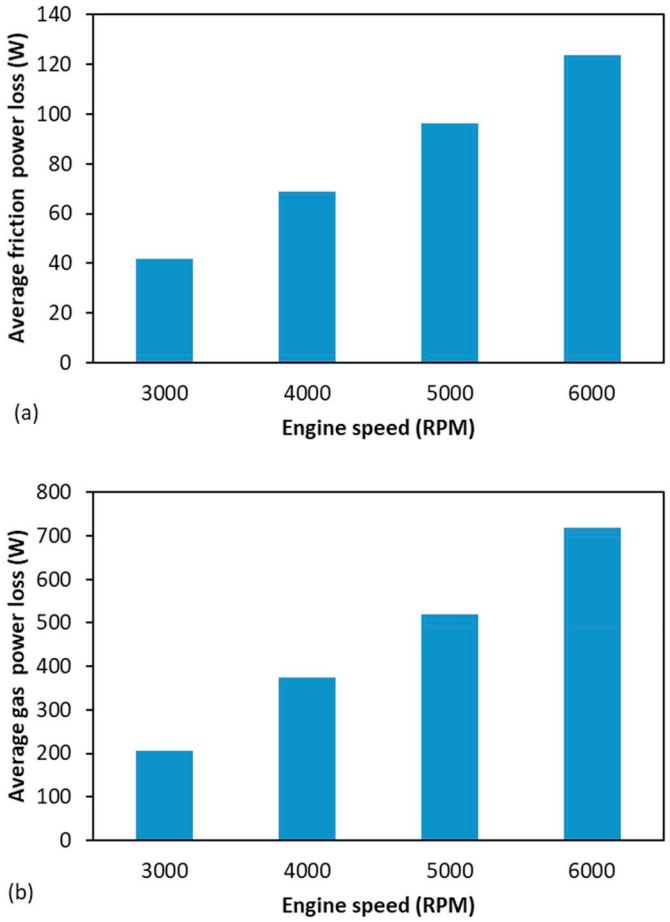


**Fig. 8.** Average power loss (a) friction (b) gas blow by.

$$W_d = \frac{\gamma_s}{(\gamma_s - 1)} RT_U \left[ 1 - \left( \frac{P_D}{P_U} \right)^{\frac{(\gamma_s - 1)}{\gamma_s}} \right] \tag{22}$$

This specific work is associated with the power losses as:

$$P_l = \dot{m} W_d \tag{23}$$

where, the mass flow rate due to gas blow-by, $\dot{m}$, is the flow rate of the gases as they flow from upstream to downstream pressure.

### 2.3. In-plane elastodynamics of compression ring

Lang [50] described the equations of motion for small deformations of curved beams as:

$$-\frac{E_2 I_2}{R_2^4}\left(\frac{\partial^3 w}{\partial \theta^3} + \frac{\partial^4 u}{\partial \theta^4}\right) + \frac{E_2 A_2}{R_2^2}\left(-u + \frac{\partial w}{\partial \theta}\right) = \rho_2 A_2 \frac{\partial^2 u}{\partial t^2} - f_R \tag{24}$$

$$\frac{E_2 A_2}{R_2^2}\left(-\frac{\partial u}{\partial \theta} + \frac{\partial^2 w}{\partial \theta^2}\right) + \frac{E_2 I_2}{R_2^4}\left(\frac{\partial^2 w}{\partial \theta^2} + \frac{\partial^3 u}{\partial \theta^3}\right) = \rho_2 A_2 \frac{\partial^2 w}{\partial t^2} - f_p \tag{25}$$

where, $\rho_2$, $I_2$, $A_2$, $R_2$ and $\theta$ are the piston ring material density, the second area moment of inertia, the cross-sectional area of the ring, the ring radius of curvature and the angular position along the ring circumference respectively. $f_R$ and $f_p$ are the radially and tangentially applied in-plane forces acting radially on the piston ring. Deflections $u$ and $w$ act in the radial and circumferential in-plane directions.

The following assumptions apply to the compression ring in-plane radial dynamics:

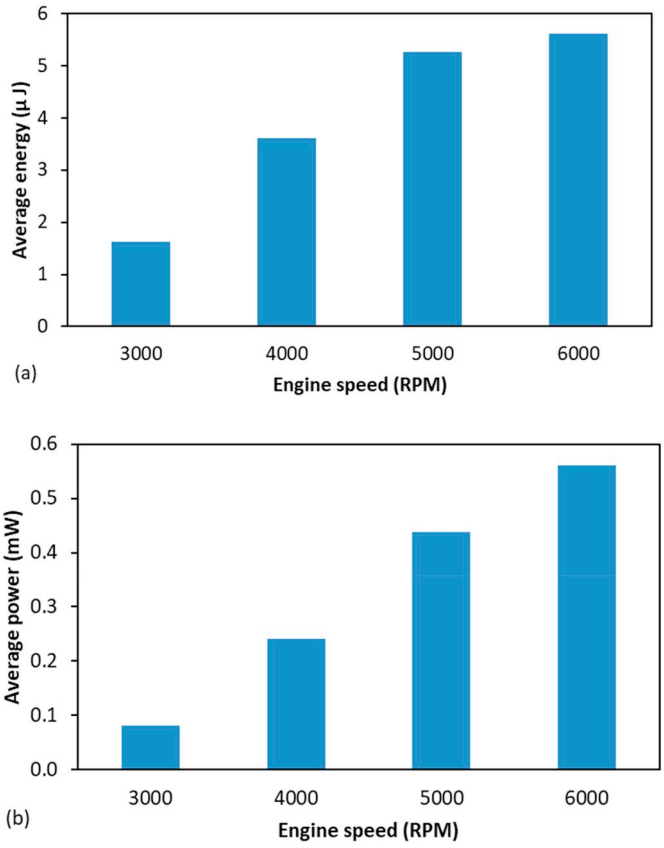


**Fig. 9.** Average ring in-plane (a) deformation energy and (b) power for one complete engine cycle.

- The effect of rotary inertia and shear deformation are negligible.
- The cross-section of the ring is invariable along all its periphery.
- The centreline of the ring follows either a full circle or a circular arc.
- Free-free boundary conditions are applied to the ring segment.

Equations (24) and (25) are discretised using the central finite difference method (FDM) [32]. The in-plane dynamic model is detailed and validated with experimental measurements in Turnbull et al. [32].

### 2.4. Method of solution

Three models are utilised in an integrated multi-physics manner in the current investigation. The first model (rigid-body ring dynamics model) deals with the tribology of piston compression ring-to-cylinder liner conjunction. This model assumes rigid body ring dynamics with the gas pressure acting behind the inner rim of the ring to be the combustion chamber pressure. In this model, the film thickness for each crank angle is obtained by considering the forces applied on the ring as well as the ring inertial force in the radial direction. The second model (flexible ring dynamics) removes the assumption of the rigid ring by including elastodynamics of the flexible ring, coupled with the tribological investigation. Thus, in this method, the ring circumferential shape and subsequently the gap between the ring and the liner can be determined through use of elastodynamics Equations (24) and (25). The third model (flexible ring dynamics and compressible gas flow) uses realistic gas pressures behind the ring, using a gas blow-by model, including the flexible ring dynamics as well as the tribological ring-liner interfacial model. The solution is depicted in the flowchart of Fig. 2.

## 3. Results and discussions

The overall multi-physics model comprises ring dynamics and its

structural modal behaviour, as well as tribology of ring-liner contact and the associated gas blow-by. Thermal effects are included in lubricant rheology as well as the compressible gas flow. Frictional heat generation and transfer through the ring-cylinder liner contact is neglected (note that the liner measured temperature is used for the analysis). Gas flow and its compressibility in the crevices consume a small portion of the fuel energy. This effect has not been investigated in the studies of power loss of this conjunction.

This paper makes a comparative study of the three methodologies: (i) with rigid-body ring dynamics, (ii) with flexible ring dynamics and (iii) with flexible ring dynamics and compressible gas flow. The predicted power loss is validated with the measured results from a motored engine test.

A single-cylinder, four-stroke, spark-ignition (SI) Honda CRF450R motocross motorbike race engine was used by Gore et al. [51,52] in a dynamometric test using an Oswald 250 kW transient dynamometer. The experimental setup and calibration are detailed in Gore et al. [51, 52]. Experimental measurements were reported under motored and fired engine conditions. It was possible to isolate the power losses specific to the compression ring conjunction under motored condition. In this case a slightly oversized piston (reduced nominal clearance) was used in the tests carried out without the presence of the compression ring (the engine has 2 rings, one compression and the other an oil control ring) In the configuration used, friction was measured directly using a floating liner [51,52]. The motored engine results are used to validate the current analysis. Engine specifications for the motored conditions are given in Ref. [51]. After validation of the methodology, the combined multi-physics approach is used to predict the power losses of the compression ring for the fired engine conditions as the compression ring cannot be removed under fired conditions. Engine specifications for the fired engine conditions are provided in Table 1.

### 3.1. Validation of numerical methodology (motored engine conditions)

Simulations are carried out for the cases of ring rigid-body dynamics, flexible ring elastodynamics and a flexible compression ring with compressible gas flow. For all these analyses the motored engine data from Gore et al. [51,52] is used. The predicted minimum film thickness is shown for these various scenarios in Fig. 3a. The horizontal lines in the figure demarcate the boundaries for hydrodynamics ($\lambda \geq 3$), mixed regime of lubrication ($1 \leq \lambda \leq 3$) and boundary regime of lubrication ($\lambda < 1$). The piston compression ring undergoes hydrodynamic regime of lubrication for a large part of the engine cycle. Asperity interactions occur at piston reversals (particularly at the top dead centre) due to a reduction in lubricant entrainment into the conjunction. The associated friction indicates that boundary interactions take place at the top dead centre in the combustion (power) stroke (Fig. 3b). Contact pressure is distributed more uniformly for the flexible ring and there is a rise in the minimum lubricant film thickness. Therefore, boundary friction is marginally mitigated with a flexible ring.

Gas flows through the piston ring to piston crevices before it settles in the piston groove. Gas pressure behind the compression ring differs from cylinder pressure due to its compressibility and temperature variations near the surfaces. This effect has not hitherto been taken into account in the open literature and constitutes one of the original contributions of the current study. Thus, the predicted boundary friction is noticeably decreased after the inclusion of gas blow-by effect (Fig. 3b). Similar trends are observed for the predicted power losses of a flexible ring and a flexible ring with compressible gas flow (Fig. 3c). The contribution of flexible ring to power losses is significant during an engine cycle. Gas compressibility effect noticeably affects the power loss during the compression stroke.

Boundary friction accounts for approximately 30% of the power losses and mainly resides around the top dead centre in transition from the compression to combustion stroke (Fig. 3b). Therefore, the predicted and measured frictions are analysed between −45 and 45° crank angles (Fig. 4a). The results show the significance of the multi-physics approach in studying piston ring problems. The rigid-body model over-estimates the frictional losses by two folds. As the complexity of the model increases through inclusion of ring flexibility and gas blow-by, the predictions converge to the measured friction from motored engine by Gore et al. [51]. Frictional losses are divided into before and after top dead centre regions in compression and power strokes (Fig. 4b and c). Contact pressure and lubricant's speed of entraining motion play significant roles in generated friction. Gas blow-by model suggests that contact pressures are lower before top dead centre. Thus, there is good agreement between the predicted and measured frictional losses. The deviation for the region past the top dead centre reversal is larger due to contact thermal effects. Numerical errors can be improved using a heat transfer model.

It is clear that the more detailed multi-physics model, including ring-liner tribological conjunction, elastodynamics of a flexible compression ring and compressible gas flow, provides more realistic predictions and conforms better to the experimental measurements of Gore et al. [52] for motored engine conditions. The results can be considered as a good validation of the integrated multi-physics methodology, which can be used to provide prediction of piston compression ring performance, which is quite difficult to isolate experimentally under the fired engine conditions.

### 3.2. Fired engine results

As it has been already noted, ring flexibility and gas blow-by significantly improve the accuracy of numerical predictions. The harsher operating conditions of fired engines suggest that friction and gas flow power losses may be quite comparable. Thus, the overall integrated model, comprising tribology of ring-liner conjunction with elastodynamics of the flexible ring and gas blow-by analysis is extended to fired engine operating conditions. Fig. 5 shows the measured cylinder pressures at various engine speeds for the same Honda CRF 450R using a Kistler 6081A40 probe by Dolatabadi et al. [53].

Mixed regime of lubrication occurs during piston reversals and especially during the combustion stroke due to the reduced sliding velocity and increased contact load, resulting in the reduction of the minimum film thickness (Fig. 6a). Lubricant film thickness increases with engine speed except during the combustion stroke as the piston approaches the mid-stroke from the top dead centre. Contact pressures are comparable for all engine speeds during large parts of the engine cycle. However, contact pressure during the piston reversal at the combustion stroke is noticeably lower at 3000 rpm in comparison with the other engine speeds. Therefore, the lubricant film can reform quicker. At 4000 rpm engine speed, lubricant film is thinner than the film at 3000 rpm due to the contact pressure effect. This trend reverses as engine speed increases above 4000 rpm. This behaviour demonstrates the careful balance needed between contact pressure and entrainment velocity. A sudden reduction in the film thickness appears during the maximum cylinder pressure.

Ring deflection (an intrusion toward the cylinder liner) at the location of the minimum film thickness is evaluated for various engine speeds (Fig. 6b). Fig. 6b suggest that ring deflection is comparable with the lubricant film thickness at the top dead centre and into the combustion stroke. This finding confirms that lubricant squeeze action is largely affected by ring flexibility.

A comparison between the results of the motored and fired engine conditions suggests that friction plays a significant role during the combustion stroke (Fig. 7a). During this part of the engine cycle, the regime of lubrication is mixed. The possibility of wear increases with the cessation of lubricant entrainment velocity during piston reversals and the power loss is exacerbated in these regions (Fig. 7b).

Fig. 8a shows the variation of power loss with engine speed. Power loss increases approximately by 82 W per cycle with the speed ramping up from 3000 to 6000 rpm. Gas flow and compressibility in piston and

piston ring crevices consume a part of the engine power (Fig. 8b). The combined analysis of frictional and gas power losses has not been reported hitherto using a flexible ring tribodynamics model. Gas power loss is up to 6 times larger than frictional power losses under fired operating conditions.

The energy associated with the in-plane deformation of the compression ring is averaged during an engine cycle (Fig. 9a). The dissipated energy is noticeable over multiple engine cycles during the lifespan of an internal combustion engine. Energy associated with deforming the ring could be conceptually harvested [54] and utilised in a power recovery system or for powering local sensors to monitor the piston system.

## 4. Concluding remarks

The paper reports on comparative studies of three compression ring models with increasing levels of complexity: (i) ring rigid-body dynamics, (ii) flexible ring dynamics and (iii) flexible ring model encapsulating gas blow-by. The contact conjunctional analyses of ring-bore are identical in all scenarios. The motored engine analyses suggest that the multi-physics nature of ring problem is fundamental to accurate prediction of friction and power losses.

The numerical predictions show that the compression ring remains in a mixed regime of lubrication during the transition from the compression stroke to the combustion stroke. The boundary friction contributions are significant before the top dead centre reversal and into the power (combustion) stroke as well as at piston reversals. Lubricant film sufficiently separates the surfaces in all mid-strokes, where the hydrodynamic regime of lubrication is dominant. Gas flow power loss can be up to six times greater than frictional losses in fired engines, caused by ring elastodynamics. This is an important original finding, not hitherto reported in literature.

Ring deflection and the minimum film thickness are comparable at the top dead centre of the combustion stroke. The associated energy and power loss to the in-plane ring deformation is evaluated, showing a significant increase in energy levels with engine speed. These findings show that the influence of flexible ring dynamics and gas blow-by on contact geometry, lubricant squeeze film action and friction prediction cannot be neglected.

Future improvements of the predictions would be possible provided the effects of lubricant starvation, film reformation and contact thermal effects are considered. The current study is focused on frictional losses and this model can be used to include the piston ring elastodynamics and gas blow-by in an accurate manner in the prediction of fuel economy, thermal effects and emissions. It would be interesting to experimentally verify the model outputs further using monitoring other performance parameters of an engines including emissions.

## Acknowledgement

The authors would like to express their gratitude to the Engineering and Physical Sciences Research Council (EPSRC) for most of the research carried out under the Encyclopaedic Program grant (EP/G012334/1) and some under the Centre for Doctoral Training (EP/L014998/1) in Embedded Intelligence (CDT-EI).

## References

[1] Andersson BS. Company perspectives in vehicle tribology - volvo. In: In tribology series, vol 18. Elsevier; 1991. p. 503–6.
[2] Castleman Jr RA. A hydrodynamical theory of piston ring lubrication. Physics 1936;7(9):364–7.
[3] Furuhama S. A dynamic theory of piston-ring lubrication 1st report, calculation. Bulletin of JSME 1959;2(7):423–8.
[4] Dowson D, Ruddy BL, Economou PN. The elastohydrodynamic lubrication of piston rings. In: Proc. royal society, A. mathematical and physical sciences. 386; 1983. p. 409–30. 1791.
[5] Jeng YR. "Theoretical analysis of piston-ring lubrication Part I—fully flooded lubrication". Tribol Trans 1992;35(4):696–706.
[6] Jeng YR. "Theoretical analysis of piston-ring lubrication Part II—starved lubrication and its application to a complete ring pack". Tribol Trans 1992;35(4):707–14.
[7] Akalin O, Newaz GM. "Piston ring-cylinder bore friction modelling in mixed lubrication regime: part I—analytical results". J Tribol 2001;123(1):211–8.
[8] Akalin O, Newaz GM. "Piston ring-cylinder bore friction modelling in mixed lubrication regime: Part II—correlation with bench test data". J Tribol 2001;123(1):219–23.
[9] Furuhama S, Sasaki S. New device for the measurement of piston frictional forces in small engines. SAE Trans.; 1983. p. 781–92.
[10] Ma MT, Sherrington I, Smith EH. Analysis of lubrication and friction for a complete piston-ring pack with an improved oil availability model: Part 1: circumferentially uniform film. In: Proc. IMechE, part j: j engineering tribology. 211; 1997. p. 1–15. 1.
[11] Mishra PC, Balakrishnan S, Rahnejat H. Tribology of compression ring-to-cylinder contact at reversal. In: Proc. IMechE, part j: j engineering tribology. 222; 2008. p. 815–26. 7.
[12] Mishra PC, Rahnejat H, King PD. "Tribology of the ring—bore conjunction subject to a mixed regime of lubrication". In: Proc. IMechE, part C: j mechanical engineering science. 223; 2009. p. 987–98. 4.
[13] Fang C, Meng X, Kong X, Zhao B, Huang H. Transient tribo-dynamics analysis and friction loss evaluation of piston during cold- and warm-start of a SI engine. Int J Mech Sci 2017;133:767–87.
[14] Rahmani R, Theodossiades S, Rahnejat H, Fitzsimons B. Transient elastohydrodynamic lubrication of rough new or worn piston compression ring conjunction with an out-of-round cylinder bore. In: Proc. IMechE, part J: J. engineering tribology. 226; 2012. p. 284–305. 4.
[15] Piao Y, Gulwadi SD. Numerical investigation of the effects of axial cylinder bore profiles on piston ring radial dynamics. J. Eng Gas Turbines Power 2003;125(4):1081–9.
[16] Tian T, Noordzij LB, Wong VW, Heywood JB. Modeling piston-ring dynamics, blowby, and ring-twist effects. J. Eng Gas Turbines Power 1998;120(4):843–54.
[17] Jackson MA. "Assessment of a sulfur dioxide based diagnostic system in characterizing real time oil consumption in a diesel engine", Doctoral Dissertation. Massachusetts Institute of Technology; 1996.
[18] Takiguchi M, Sasaki R, Takahashi I, Ishibashi F, Furuhama S, Kai R, Sato M. Oil film thickness measurement and analysis of a three ring pack in an operating diesel engine. SAE Technical Paper; 2000. 2000-01-1787.
[19] Baelden C, Tian T. A dual grid curved beam finite element model of piston rings for improved contact capabilities. SAE Int. J. Engines 2014;7(1):156–71.
[20] Baker CE, Theodossiades S, Rahnejat H, Fitzsimons B. Influence of in-plane dynamics of thin compression rings on friction in internal combustion engines. J Eng Gas Turbines Power 2012;134(9):092801.
[21] Baker C, Rahmani R, Theodossiades S, Rahnejat H, Fitzsimons B. On the effect of transient in-plane dynamics of the compression ring upon its tribological performance. J Eng Gas Turbines Power 2015;137(3):032512.
[22] Baker C, Theodossiades S, Rahmani R, Rahnejat H, Fitzsimons B. On the transient three-dimensional tribodynamics of internal combustion engine top compression ring. J Eng Gas Turbines Power 2017;139(6):062801.
[23] Xu Y, Zheng Q, Geng J, Dong Y, Tian M, Yao L, Dearn KD. Synergistic effects of electroless piston ring coatings and nano-additives in oil on the friction and wear of a piston ring/cylinder liner pair. Wear 2019;422:201–11.
[24] Peng Y, Xu Y, Geng J, Dearn KD, Hu X. Tribological assessment of coated piston ring-cylinder liner contacts under bio-oil lubricated conditions. Tribol Int 2017;107:283–93.
[25] Furuhama S, Hiruma M, Tsuzita M. Piston ring motion and its influence on engine tribology. SAE Trans 1979:2929–41.
[26] Namazian M, Heywood JB. Flow in the piston-cylinder-ring crevices of a spark-ignition engine: effect on hydrocarbon emissions, efficiency and power. SAE Trans.; 1982. p. 261–88.
[27] Baker CE, Rahmani R, Karagiannis I, Theodossiades S, Rahnejat H, Frendt A. Effect of compression ring elastodynamics behaviour upon blowby and power loss. SAE Technical Paper; 2014. 2014-01-1669.
[28] Ejakov MA, Schock HJ, Brombolich LJ. Modeling of ring twist for an IC engine. SAE Trans; 1998. p. 2284–98.
[29] Tian T. Dynamic behaviours of piston rings and their practical impact. Part 1: ring flutter and ring collapse and their effects on gas flow and oil transport. In: Proc. IMechE, part j: j. engineering tribology. 216; 2002. p. 209–28. 4.
[30] Tian T. Dynamic behaviours of piston rings and their practical impact. Part 2: oil transport, friction and wear of ring/liner interface and the effects of piston and ring dynamics. In: Proc. IMechE, part j: j engineering tribology. 216; 2002. p. 229–48. 4.
[31] Turnbull R, Mohammadpour M, Rahmani R, Rahnejat H, Offner G. Coupled elastodynamics of piston compression ring subject to sweep excitation. In: Proc. IMechE, part K: j multi-body dynamics. 231; 2017. p. 469–79. 3.
[32] Turnbull R, Rahmani R, Rahnejat H. In-plane and out-of-plane elastodynamics of thin rings and seals. J Comput Nonlinear Dyn 2019. https://doi.org/10.1115/1.4043526.
[33] Rahnejat H. Multi-body dynamics: vehicles, machines, and mechanisms. Bury St Edmunds, UK: Professional Engineering Publishing; 1998.
[34] Dowson D, Higginson GR. A numerical solution to the elasto-hydrodynamic problem. J Mech Eng Sci 1959;1(1):6–15.

[35] Yang P, Cui J, Jin ZM, Dowson D. Transient elastohydrodynamic analysis of elliptical contacts. Part 2: thermal and Newtonian lubricant solution. In: Proc. IMechE, part j: j engineering tribology. 219; 2005. p. 187–200. 3.
[36] Houpert L. New results of traction force calculations in elastohydrodynamic contacts. J Tribol 1985;107(2):241–5.
[37] Roelands CJ. "Correlational aspects of the viscosity-temperature-pressure relationship of lubricating oils", Doctoral Thesis. Technische Hogeschool te Delt; 1966.
[38] Greenwood JA, Tripp JH. The contact of two nominally flat rough surfaces. In: Proc. IMechE, J mech eng sci. 185; 1970. p. 625–33. 1.
[39] Teodorescu M, Balakrishnan S, Rahnejat H. Integrated tribological analysis within a multi-physics approach to system dynamics. In Tribology and Interface Engineering Series 2005;48:725–37.
[40] Styles G, Rahmani R, Rahnejat H, Fitzsimons B. "In-cycle and life-time friction transience in piston ring–liner conjunction under mixed regime of lubrication". Int J Engine Res 2014;15(7):862–76.
[41] Eyring H. Viscosity, plasticity, and diffusion as examples of absolute reaction rates. J Chem Phys 1936;4(4):283–91.
[42] Leighton M, Nicholls T, De la Cruz M, Rahmani R, Rahnejat H. "Combined lubricant–surface system perspective: multi-scale numerical–experimental investigation". In: Proc. IMechE, part j: j engineering tribology. 231; 2017. p. 910–24. 7.
[43] Morris N, Rahmani R, Rahnejat H, King PD, Fitzsimons B. Tribology of piston compression ring conjunction under transient thermal mixed regime of lubrication. Tribol Int 2013;59:248–58.
[44] Ma Z, Henein NA, Bryzik W. A model for wear and friction in cylinder liners and piston rings. Tribol Trans 2006;49(3):315–27.
[45] Rahmani R, Rahnejat H, Fitzsimons B, Dowson D. The effect of cylinder liner operating temperature on frictional loss and engine emissions in piston ring conjunction. Appl Energy 2017;191:568–81.
[46] Furuhama S, Tada T, Nakamura T. Some measurements of the piston temperatures in a small type gasoline engine. Bulletin of JSME 1964;7(26):422–9.
[47] Theaker M, Rahmani R, Rahnejat H. Prediction of ring-bore conformance and contact condition and experimental validation. In: ASME 2012 internal combustion engine division spring technical conference; 2012. p. 885–92.
[48] Sutherland W. "The viscosity of gases and molecular force", London Edinburgh Dublin Philos. Mag. J. Sci. 1893;36(223):507–31.
[49] Woods WA. On the role of the harmonic mean isentropic exponent in the analysis of the closed-cycle gas turbine. Proc.IMechE, Part A: J. Power and Energy 1991; 205:287–91. 4.
[50] Lang TE. "Vibration of thin circular rings, Part 1", jet propulsion laboratory. Pasadena, CA: California Institute of Technology; 1962. p. 32–261. Technical Report.
[51] Gore M, Rahmani R, Rahnejat H, King PD. Assessment of friction from compression ring conjunction of a high-performance internal combustion engine: a combined numerical and experimental study. In: Proc. IMechE, part C: j mech eng sci. 230; 2016. p. 2073–85. 12.
[52] Gore M, Theaker M, Howell-Smith S, Rahnejat H, King PD. Direct measurement of piston friction of internal-combustion engines using the floating-liner principle. In: Proc. IMechE, part D: j. automobile engineering. 228; 2014. p. 344–54. 3.
[53] Dolatabadi N, Littlefair B, De la Cruz M, Theodossaides S, Rothberg SJ, Rahnejat H. A transient tribodynamics approach for the calculation of internal combustion engine piston slap noise. J Sound Vib 2015;352:192–209.
[54] Zhang XF, Hu KM, Li H. Comparison of flexoelectric and piezoelectric ring energy harvester. In: Proc. IMechE, part C: j mech eng sci; 2018. 0954406218806018.